1

TEXTILE ANTENNAS FOR BODY AREA NETWORKS: DESIGN STRATEGIES AND EVALUATION METHODS

PING JACK SOH[1] AND GUY A. E. VANDENBOSCH[2]

[1] *Advanced Communication Engineering Centre, School of Computer and Communication Engineering, Universiti Malaysia Perlis, Arau, Perlis, Malaysia*
[2] *ESAT-TELEMIC Research Division, Department of Electrical Engineering, KU Leuven, Leuven, Belgium*

1.1 INTRODUCTION

Due to the increasing demand for multi-functional, multi-band wireless operation and consumer-centric technology, textile antennas have been receiving growing attention [1]. Future wearable systems should be unobtrusive, flexible, and operating with minimal degradation in proximity to the human body. These antennas have to meet the bandwidth, efficiency, and safety requirements, while being consistent with low-cost manufacturing techniques. Moreover, in wearable applications, flat surfaces cannot be guaranteed. Thus, an important antenna requirement is its ability to work with good robustness against environmental, positional, and location changes when being worn, besides complying with medical and safety regulations.

Body-centric antennas are crucial in catering for various current and future wireless standards. Among others, wearable antennas could assist medical monitoring for hospitalized, homebound, or outpatients [2, 3]. They could be applied in emergency service communication and public safety support (e.g., firefighters) [4–6]. They could

Electromagnetics of Body-Area Networks: Antennas, Propagation, and RF Systems, First Edition.
Edited by Douglas H. Werner and Zhi Hao Jiang.

also provide flexibility in assisting communication in search, rescue, and location-tracking alerts, especially in hazardous environments [7, 8]. There is also the possibility that they will become popular in consumer electronics in the near future, applied for communication [9], positioning, and navigation for recreational purposes [10].

Wearable antennas are electrical radiators being made flexible enough to be worn and to work in the proximity of a user's body. Since it is ergonomically more suitable that a wearable antenna for Wireless Body Area Networks (WBAN) applications is flexible and made to conform to the body, it is only natural that textiles be used to achieve these requirements compared to conventional metallic structures, for example, rigid copper plates or tapes which are worn. However, degradation of the antenna performance when worn on the human body has been one of the major deterrents in its successful implementation, be it in terms of frequency detuning, bandwidth reduction, and efficiency degradation or radiation distortion [11]. In other words, ideally, a wearable antenna must be designed to be immune enough for an on-body operation. Moreover, a flexible antenna made from textile is regarded as a realistic candidate due to the advancements in conductive textiles and the ergonomic properties that it is able to offer. Since these textiles are either newly introduced or have been traditionally used for other purposes, for example, electromagnetic interference (EMI) shielding or grounding, one of the important and yet challenging aspects of this work is to properly characterize their electrical properties at the intended frequencies.

In this chapter, firstly, a brief overview of the types of textiles (conductive and non-conductive) is given. Next, the characterization procedure using a commercial setup is explained prior to the proposal of a systematic antenna fabrication procedure. Finally, this chapter also describes the evaluation methods used for the fabricated antenna prototypes, that is, in terms of reflection coefficient, radiation characteristics, efficiency, and specific absorption rates (SAR).

1.2 TEXTILE MATERIALS AND ANTENNA FABRICATION PROCEDURE

Textile antenna prototyping materials generally consist of two textile types, conducting and non-conducting. The former is typically used to form antenna conductive elements (radiator, ground plane, shorting wall, etc.), whereas the latter is used to form the substrate, spacer, etc. For example, in the case of a Planar Inverted-F Antenna (PIFA) topology, conductive textiles are used as its radiator, ground plane, and shorting wall, whereas felt or fleece is used as the substrate. The properties of several popular commercial off-the-shelf textiles can be found in [4] and [12–14], and will be explained in the following sections.

1.2.1 Conductive Textiles/Foils

Initially, flexible antennas are prototyped using copper foil, as this is flexible and a rough representation of a textile antenna. However, the introduction of electrically conductive acrylic adhesives which are reasonably homogeneous in terms of surface

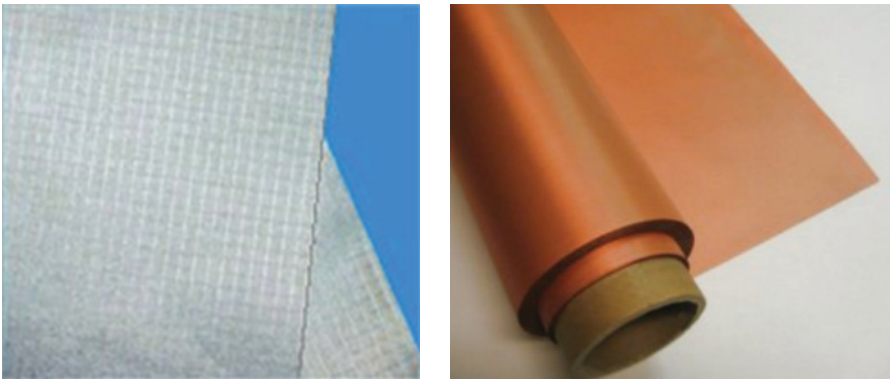

(a) (b)

FIGURE 1.1 Conductive textiles: (a) ShieldIt Super [15] and (b) PCPTF [16]. Used with permission from LessEMF.com.

resistivity/conductivity and mechanically stable has eased the fabrication of antennas made using commercial off-the-shelf textiles. These materials can be used as the radiating or grounding element for a textile antenna, and are required to be highly conductive, with surface resistivities (R_s) of less than 0.05 Ω/sq.

Three of the more popular conducting materials for wearable antennas are described as follows and are shown in Figure 1.1

(a) Copper foil tape: a 0.035 mm thick foil, coated with a 0.03 mm thickness.
(b) ShieldIt Super [15]: a ripstop, woven polyester textile coated with copper and nickel. Its thickness is 0.17 mm and its estimated weight is 230 g/m^2.
(c) Pure copper polyester taffeta fabric (PCPTF) [16]: plain woven and coated using pure copper. It has a thickness of 0.08 mm and an estimated weight of 80 g/m^2.

The parameter of prime importance is the equivalent conductivity of the textile used. This parameter ultimately determines the losses, and consequently, the efficiency and gain of the antennas. The homogenized conductivities were calculated based on the surface resistances provided by the manufacturer. The thickness of the conductive textile can be chosen depending on the application and location of the on-body deployment. For example, if the antennas are needed for health monitoring of the aged, thinner and low-cost materials may be chosen as they might be less exposed to harsh environments compared to the use of such antennas in military applications.

1.2.2 Non-conductive Textiles

The substrates used to fabricate wearable textile antennas are generally chosen to enable ease of integration onto the users' clothing. Upon the selection of a suitable textile substrate, it is important that its permittivity and loss tangent are characterized

via measurements. Note that material properties for the same substrate might differ due to (small) variations in the fabrication process. For example, it is found that for felt [17], values given in literature are within the following ranges: ε_r in between 1.18 [18] and 1.45 [19], and δ_{tan} in between 0.004 [18] and 0.025 [14]. This illustrates that a proper measurement of felt characteristics is still necessary. On the other hand, measurements using an in-house developed technique based on the cavity method yielded a relative permittivity of $\varepsilon_r = 1.45$, and $\delta_{tan} = 0.044$ at 2.45 GHz. Another example is the polyester fleece [20], a soft napped insulating fabric made from synthetic fibers. Such material is typically used to manufacture loss tangent jackets, hats, pants, sweaters, gym clothes, and high-performance outdoor clothing [21]. Its reported permittivity ranges from 1.04 [7, 22] to 1.25 [23], and none of the publications reported the characterization of its loss tangent.

1.2.3 Textile Antenna Fabrication Procedure Using Commercial Textiles

Fabrication starts by cutting a single piece of textile or copper foil according to the designed and optimized shape. Then, the textile is folded over and fastened on the felt fabric to form the antennas. Depending on the antenna topology, a sufficiently large hole for the insertion of a 50 Ω SMA connector is needed. This is mainly to avoid shorting contacts between the radiator and the ground plane, once soldering or conductive epoxy is applied. Fastening copper foil and ShieldIt textile to the substrate is simpler, as both materials come with adhesive reverse sides. ShieldIt comes with a heat-activated reverse side adhesive, which is firm and typically enables it to be secured accurately onto substrates. On the other hand, it should be noted that the contact between the copper foil adhesive and the non-woven felt substrate degrades with time, thus the use of additional non-conductive adhesive is highly recommended. Although this might slightly affect the overall material thickness and its electrical properties, more adverse effects are expected as the original adhesive degrades and as the copper foil edges peel off and lift up, allowing the existence of air gaps. PCPTF, on the other hand, has to be stitched onto the substrate along its perimeter. This almost always results in an uneven conductive surface around the antenna perimeter, at locations where the conductive surface is sewn to the substrate layer. Besides, manual stitching, if not carefully done, could also result in misalignments. Thus it is also recommended that a small amount of non-conductive adhesive be applied prior to the stitching process. Meanwhile, to ensure proper electrical connection between PCPTF textile and the SMA connector, a silver conductive epoxy model 8331 from MG Chemical is used. Fabrication using this simple method provides an estimated accuracy of about 0.2 mm [12].

To realize a full textile fabrication, several high-level requirements are imposed.

(a) The whole structure or structure on the same layer has to be fabricated out of a single piece of textile. This avoids additional interconnections using glue/epoxy and maintains a consistent surface conductivity.

(b) The structure has to be simple and as symmetrical as possible, to ease fabrication.

(c) Hard-to-cut shapes/corners should be avoided to minimize fabrication inconsistencies.

1.3 DESIGN STRATEGIES AND EVALUATION METHODS

1.3.1 Antenna Simulation and Evaluation in Free Space

Similarly as for a conventional antenna, it is crucial that the performance of a textile antenna is first evaluated using a numerical electromagnetic solver. Such antenna is typically designed using a series of design equations, resulting in a set of initial dimensions. The general input parameters to these equations are the operational frequency, bandwidth, and permittivities and loss tangents of the materials. For this reason, it is important that the material properties are determined using the most accurate method available to the antenna designer. This is to ensure that the performance predicted by the antenna is not affected by a mischaracterization of the materials.

Textile substrates can be inserted in simulators in exactly the same way as conventional substrates: in most cases, the conductive textiles are defined as a lossy metal. This simplifies the analysis. For example, the two conductive textiles introduced earlier are defined with an estimated conductivity of $\sigma_S = 1.18 \times 10^5$ S/m for ShieldIt and $\sigma_P = 2.5 \times 10^5$ S/m for PCPTF, using the approximate equation proposed in [24], as follows:

$$\sigma = \frac{1}{R_s \cdot t} \tag{1.1}$$

where σ is the conductivity (S/m), R_s is the surface resistance (Ω/sq), and t is the thickness of the conductive textile (m). The copper foil conductivity is simplified as $\sigma_C = 5.88 \times 10^7$ S/m, assuming that the conductivity of the adhesive is negligible.

Further, it is also important to properly understand how the simulator operates to ensure the most accurate results. Most simulators are categorized according to the method used to solve Maxwell's equations, either in time or frequency domain. Several numerical techniques exist: the finite integration technique (FIT) [25, 26], the finite-difference time-domain (FDTD) [27–30], the transmission line matrix (TLM) method [31, 32], the finite element method (FEM) [33, 34], and the method of moments (MoM) [35]. All methods involve a discretization of the entire analysis space, except for the MoM, which only discretizes the antenna itself. The computational effort for volume-based methods depends on the volumetric size, which must always be made finite. To this goal, boundary conditions are introduced. Absorbing boundary conditions are used to represent the continuous flow of energy in free space; electrically conducting walls are used for closed boxes, or periodic boundary conditions are used to represent periodic structures. Symmetries can be taken advantage of in many simulators.

The optimal simulation strategy works as follows. First, the antennas are simulated using coarse meshes across a larger frequency range. In this way computational

resources are more efficiently used, as the initial antenna performance is already predicted with a limited simulation time. Several optimization iterations are then necessary to ensure that the antenna is operating at the targeted frequency. The simulated frequency range can then be narrowed down, and a more detailed mesh can then be defined. For more exotic antenna topologies, it is important to understand the structure well via parameter sweeps.

In experiments, measurement of the reflection coefficient is performed using a vector network analyzer (VNA), whereas radiation characteristics, that is, patterns, gain, and efficiency are evaluated in an anechoic chamber. For reflection coefficient measurements, the VNA is first calibrated using the well-known short–open–load method to remove any systematic errors (losses, reflections, and phase delays) resulting from connectors, cables, and transitions. Measurement repeatability is first validated, and at least three measurements are averaged to deliver the final reflection coefficient for each antenna.

Radiation patterns are measured with the antenna under test (AUT) as the receiving antenna. A transmitting broadband antenna is placed in the far-field region of the AUT. Received power from two orthogonal AUT axes is evaluated from $-180°$ to $+180°$, before the transmitting antenna is turned to the other orthogonal polarization. This measurement sequence is then repeated, resulting in four main readings, co- and cross-polarization in *E*- and *H*-plane for a linearly polarized textile antenna. Antenna gains are measured using the widely accepted gain transfer method [36], based on the Friis transmission equation. In this method, a two-step procedure is performed. Received power is first evaluated using a standard gain antenna as the receiving antenna. This results in the following equation

$$P_{\mathrm{rREF}} = P_{\mathrm{T}} + G_{\mathrm{T}} + G_{\mathrm{rREF}} - L_{\mathrm{S}} \ \ (\mathrm{dB}) \tag{1.2}$$

where P_{rREF} is the received power at the reference antenna, G_{T} is the gain of the transmitting antenna, G_{rREF} is the known gain of the receiving reference antenna and L_{S} is the free space path loss. The receiving reference antenna is then replaced with the AUT, and the received power is measured, resulting in

$$P_{\mathrm{rAUT}} = P_{\mathrm{T}} + G_{\mathrm{T}} + G_{\mathrm{rAUT}} - L_{\mathrm{S}} \ \ (\mathrm{dB}) \tag{1.3}$$

where P_{rAUT} is the received power at the AUT and G_{rAUT} is the gain of the receiving AUT. Subtracting (1.1) from (1.2), the desired G_{rAUT} can then be calculated as

$$G_{\mathrm{rAUT}} = P_{\mathrm{rAUT}} - P_{\mathrm{rREF}} + G_{\mathrm{rREF}} \ \ (\mathrm{dB}) \tag{1.4}$$

1.3.2 On-Body Co-simulations and Experimental Evaluations

Since the proposed antennas are designed to be worn, it is crucial that they are evaluated when mounted on the human body. For wearable antennas, the focus mounting area is on the upper human torso as it is the largest and most suitable location. This is because antennas placed in this area are less prone to bending or other deformations.

Moreover, in health monitoring applications, for example, this is the location where many physiological parameters can be gathered in a non-obtrusive way. Nonetheless, in general, on-body investigations should consider several aspects such as the effect of on-body mounting locations, antenna orientations, and distances from the body.

The simplest step to predict on-body detuning is to co-simulate and further optimize the antenna in proximity of a human phantom. This will enable the antenna performance changes to be forecasted, and the designer can ensure that the antenna remains operational when placed on the body despite the coupling with the body. As the body is composed of different tissues with different material properties, the choice of a proper body phantom is critical in ensuring a good tradeoff between simulation accuracy and complexity. Moreover, tissue properties vary with frequency, while the tissue composition also depends on the body part where the antenna is to be placed. In general, body models can be categorized as either homogeneous or heterogeneous. The former generally indicates that the model is filled using a simplified, single tissue property, or an average of several tissue properties, whereas a heterogeneous model consists of a large number of tissues and a voxel resolution. Examples are found in [37] and [38] where the phantom is defined from a two-third muscle equivalent material. The dielectric properties of the tissues involved are obtained via *in vivo* measurements on human or autopsy materials. A compromise between the homogeneous and heterogeneous models is the three-layer model as illustrated in Figure 1.2 [39].

The main parameter of concern in determining the level of on-body detuning is the distance between the antenna and the body. In simulations, this can be controlled quite accurately. On the contrary, this is not the case in experiments, especially when the antenna is very flexible. Foams with different thicknesses are typically used to consistently space the antenna at a certain distance from the user's body. To maintain consistent antenna mounting location and cable routing during the on-body experiments, a custom-modified fleece jacket routed with sewn-in RF cables can be utilized. For example, in [40], two 40 cm long cables were mounted vertically on the jacket on the front and the back, connected to the AUT at one end, and to the VNA or radiation pattern measurement system at the other end. Throughout the course of this work, four placement locations were evaluated, that is, the chest, back, shoulder, and on the elbow in bent conditions. However, only two antenna mounting locations

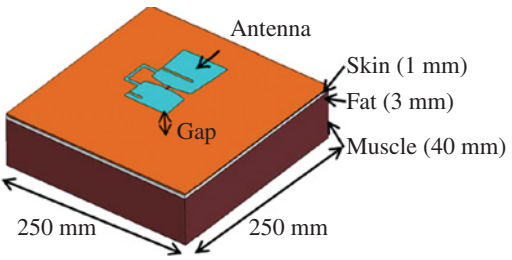

FIGURE 1.2 The three-layered human body model as defined in Wang et al. 2014 [39]. Reproduced with permission of IEEE.

FIGURE 1.3 Examples of on-body mounting locations, horizontally and vertically: (a) on the chest at 10 mm distance, (b) on the back at 10 mm distance, (c) on the chest at 0 mm distance, and (d) on the back at 0 mm distance. *Source:* Soh et al. 2012 [40]. Reproduced courtesy of The Electromagnetics Academy.

on the upper human torso (i.e., chest and back) were tested for all antennas due to the difficulty in ensuring a consistent antenna bending condition and placement position for two other locations: on the shoulder and elbow. Moreover, these two locations are less likely to be favorable for use in practice, since the antenna performances are inconsistent when operating in a bent condition. Furthermore, the substrate thickness of at least 3 mm and the felt material properties enable bent antennas to quickly regain its original planar form. To ensure antenna placement precision, two holes were created at a fixed location horizontally and vertically from the top edge of the jacket, see Figure 1.3. Measurements of reflection coefficient or radiation characteristics can be performed in an anechoic chamber using real human volunteers of different genders, heights, and weights.

Several on-body measurement configurations are illustrated in Figures 1.3a and 1.3b. For each location, the antennas are tested in both vertical and horizontal settings, with its ground plane mounted about 10 mm from the body and its radiator facing outward, away from the body. Besides the user's preference factor—whether he/she is more comfortable in tighter/looser clothing—the choice of the chest and back for this evaluation defines two locations with distinct gap sizes. In other words, clothes

are relatively closer to the chest and slightly distant from the back when a user is standing or walking, for instance. With the additional clothing worn under a jacket, it is reasoned that a 10 mm gap would be a realistic implementation. Taking into account the possibility of a simultaneous change in orientation and spacing distance caused by the users' movement, two additional configurations can be introduced to simulate a worst-case scenario: the antenna facing upward, with the substrate touching the user's clothing, as shown in Figures 1.3c and 1.3d.

1.3.3 Deformation Study

Another important component of textile antenna evaluation is studying its deformation. Such situations easily occur when a flexible or thin textile antenna is worn on the body. Deformations can be generally decomposed into

- Bending
- Crumpling
- Stretching
- Displacement

It is important for a textile antenna designer to model and evaluate these deformations in the design stage to be able to predict the practical applicability of the antenna. These investigations aim to capture the impact of instability in the antenna parameters because of variations in, for instance, the amount of antenna bending. Bending can be modeled by most electromagnetic solvers available today. They are mainly influenced by the following factors:

1. the movements or activities of users wearing the antennas
2. the variations in body morphology of the users

In a typical bending study, the textile antenna is first evaluated in its flat form prior to the evaluation of a number of bending radii. These radii need to be realistic and representative of the actual on-body placement location: on thighs, arms, neck, etc. The study has to be performed for two orthogonal bending axes, for example, the y-axis and x-axis, of a z-pointing planar antenna; see Figure 1.4. This is to ensure that the effect of bending in either of the two orthogonal planes is fully predicted.

Antennas which are easily deformed must also be experimentally evaluated. This can be done by placing them either onto a human phantom or directly onto a real human arm; see Figure 1.5. For the former, a cylindrically shaped container is typically required. This container is filled with proper tissue simulating liquid. While these liquids are commercially available, it is also possible to fabricate them using a series of chemicals. A sample of the fabricated phantom at 2.45 GHz is shown in Figure 1.6.

Due to the randomness of a user's activity and the various possible on-body placement locations, any textile antenna integrated on a worn garment may also suffer

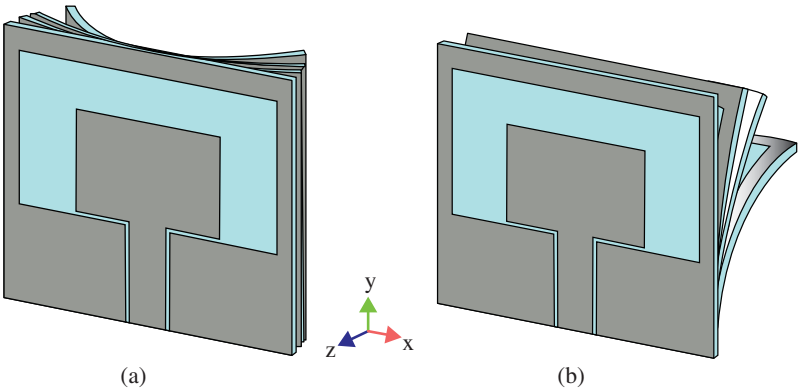

FIGURE 1.4 Modeling bending in the two orthogonal planes. *Source:* Bai and Langley 2009 [41]. Reproduced with permission of IEEE.

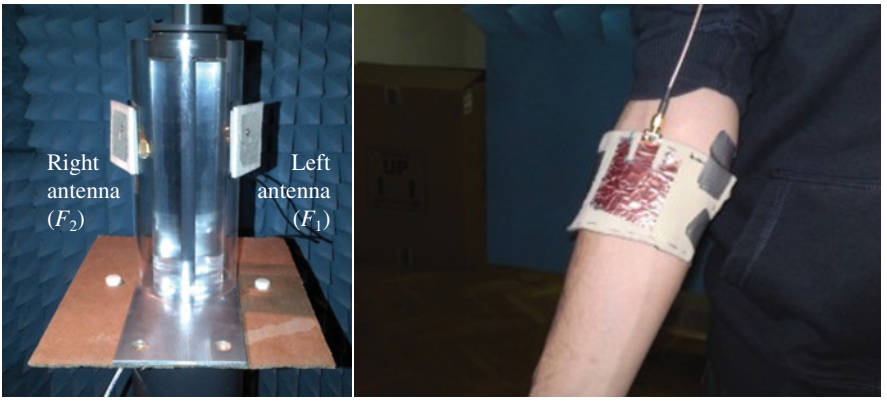

FIGURE 1.5 On-body evaluation of bending on a human phantom and on a human volunteer. *Source:* Ivsic et al. 2013 [42] and Soh et al. 2013 [43]. Reproduced with permission of IEEE.

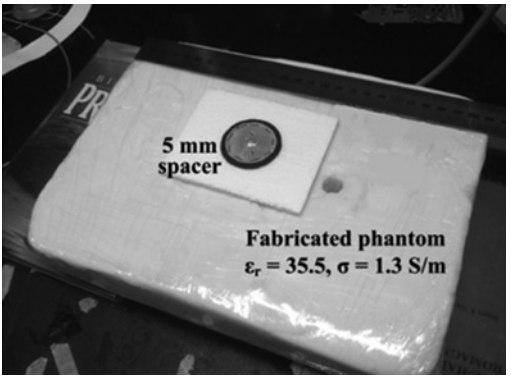

FIGURE 1.6 Fabricated sample of a semi-solid phantom. *Source:* Choi et al. 2015 [44]. Reproduced with permission of IEEE.

TABLE 1.1 The effect of crumpling on the dimensions of a sample dipole antenna [45].

	Antenna length (mm)	h (mm)	l (mm)
Flat	140	N/A	N/A
Crumpling case 1 (CC1)	133.24	11	40
Crumpling case 2 (CC2)	115.19	11	18
Crumpling case 3 (CC3)	90.23	11	10
Crumpling case 4 (CC 4)	79.28	11	8

from crumpling. A series of crumpling models is illustrated in Figure 1.7. Crumpling can be most detrimental since it reduces the electrical dimensions of the antenna. It generally results in an upward shift of the operational frequency band, and leads to an increased mismatch. This is illustrated in Table 1.1. When placed on body, it is noticed that the frequency shift is dependent on the level of the crumpling. For example, in [45], for antenna CC4, the frequency shifted upward by the largest rate, followed by CC3, CC2, and CC1. Remarkable is that matching for all crumpling cases improved at the detuned frequency; see Figure 1.8.

1.3.4 Antenna Efficiency Evaluation

Generally, since it is the easiest, the efficiency of an antenna is evaluated using numerical simulators. However, there are several methods for experimental efficiency assessment. One of the more popular methods is using a reverberation chamber (RC). Thanks to the larger size of such a chamber, a real human volunteer can be located inside the chamber while the AUT is placed on the body, either in a flat or a bent position. A reverberation chamber is typically constructed from galvanized steel and many are fit with two principle sets of mechanical stirring paddles. They are configured to be able to stir fields orthogonally throughout the volume of the chamber. One set can be mounted about a central rotational shaft from the floor to the roof and

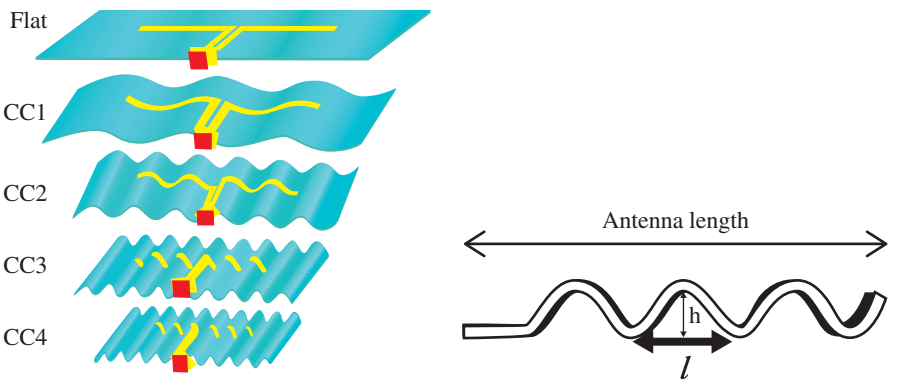

FIGURE 1.7 Modeling crumpling on a sample dipole antenna. *Source:* Elias et al. 2013 [45]. Reproduced with permission of IEEE.

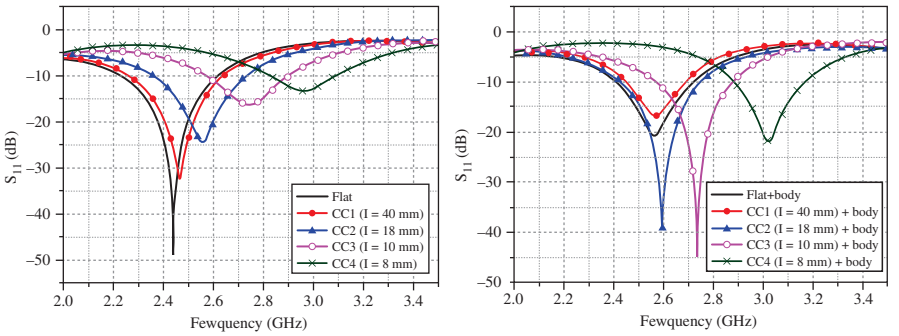

FIGURE 1.8 The effect of crumpling in free space and on the body for the case of a dipole. *Source:* Elias et al. 2013 [45]. Reproduced with permission of IEEE.

situated toward one corner of the chamber, the other set can be mounted about a rotational shaft from the front to the back wall at ceiling height. Figure 1.9 illustrates this chamber configuration. Further, as a representative example, the RC at the University of Liverpool as used in the investigations of [46–48] is described.

The physical interpretation of each stirring sequence can be briefly summarized as follows [49–51]:

(a) Mechanical stirring is the rotation or movement of electrically large paddles situated inside the chamber which change the boundary conditions of the electromagnetic field inside upon each increment.

(b) Polarization stirring requires the variation of the source (transmit) polarization to encompass both vertical and horizontal linear polarizations (in this case). It is required to ensure that no bias exists in the amount of TM and TE modes which are excited. This means that the average power level in the

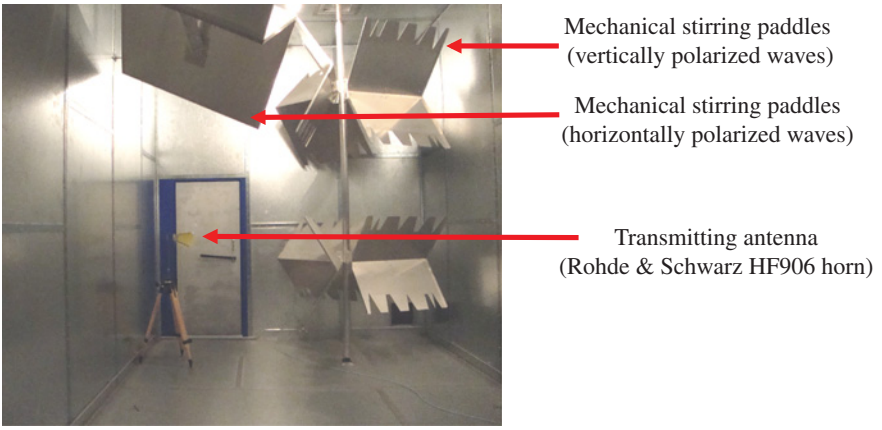

FIGURE 1.9 The RC at the University of Liverpool dimensioned at 3.6 m (width), 5.8 m (length), and 4 m (height). *Source:* Boyes et al. 2012 [46], Boyes et al. 2012 [47], and Boyes et al. 2013 [48]. Reproduced with permission of IEEE.

TABLE 1.2 RC measurement parameters at the University of Liverpool [46–48].

Parameter	Description
Frequency range	2–7 GHz
Frequency points	1601
Stirring sequences	5° mechanical stirring 2 × (orthogonal) polarization stirring 5 × position stirring 100 MHz frequency stirring
No. of measured samples	710 per frequency sample
Transmitting antenna (fixed)	Rohde & Schwarz HF906 horn
Reference antenna	Satimo SH2000 horn

measurements can be more accurately formed irrespective of the receive antennas' polarization.

(c) Position stirring is the physical movement of the AUT to various locations inside the chamber, movement distances are typically of the order of $\lambda/2$ in order to create independent samples.

(d) Frequency or electronic stirring is performed by taking a further average to effectively 'smooth' any measured results. This is usually applied in the post processing stage.

The measurement parameters used in the investigation are detailed in Table 1.2. The stirring sequences detailed in the table have been configured because

(a) a large number of measured samples (a percentage of which should be statistically independent) are required to keep the uncertainty at an acceptable level;

(b) the sequences have to be organized in such a way that the human subject does not have to spend prolonged amounts of time in the chamber to complete each measured sequence (i.e., the subject could take regular breaks if required).

All these stirring sequences (from a field perspective) are used in order to create a statistically isotropic and homogeneous field distribution in the cavity as long as the test location is situated approximately $\lambda/2$ from the walls [46–48]. The distance from the walls advocates the establishment of a "calibrated area" in which the statistically isotropic and homogeneous field distribution should be demonstrated.

As with any efficiency measurement in the RC, a reference measurement is required for calibration purposes. This was performed using a reference antenna with known efficiency values and with the preferred unidirectional pattern. Throughout the reference measurements, a human subject was located inside the chamber with the AUT located on the chest via a rigid cable terminated with a 50 Ω load. The human subject in the chamber during the reference measurement is expected to significantly load the chamber, and serves as the dominant contributor to the loss mechanisms that exist. Therefore any calibration without the human loading would simply not be accurate. Figure 1.10 illustrates the measurement setup used throughout the

FIGURE 1.10 Measurement setup of Table 1.2. *Source:* Boyes et al. 2013 [48]. Reproduced with permission of IEEE.

efficiency investigation, including reference measurements. Standard Velcro straps have been employed to hold the antenna against the human test subject. The straps themselves have not been directly touching the antenna element, but have been only used to secure the attached cable against the human subject, sufficiently holding the antenna in place to prevent any movement. The contents inside the human subject's pockets were kept constant (without mobile phone, coins, etc.) to ensure consistency. The distance between the consecutive locations shown in Table 1.3 was such that each location was positioned further than the correlation distance (of about $\lambda/2$) to create independent samples. Further, throughout all position stirring locations (for both the reference and AUT measurements), the separation between the human subject and the reference antenna was always kept a prescribed distance apart ($\gg\lambda/2$) to avoid any coupling issues that could potentially corrupt any measurement results.

As defined by the IEEE, the radiation efficiency (η_{rad}) is the "Ratio of total radiated power to the net power accepted by the antenna at its terminals." Mathematically, when measured in an RC, the radiation efficiency can be deduced from (1).

$$\eta_{\text{rad}} = \left\{ \frac{\langle |S_{21\text{AUT}}|^2 \rangle}{\langle |S_{21\text{REF}}|^2 \rangle} \times \frac{(1-(S_{22\text{REF}})^2)}{(1-(S_{22\text{AUT}})^2)} \right\} \times \eta_{\text{REF}} \tag{1.5}$$

TABLE 1.3 Position stirring locations in the RC with a minimum distance of 8 λ (at 2 GHz) from walls or other objects [48].

Position	Location
1	1.2 m from left wall
2	1.15 m from right wall, 1.1 m from stirrers
3	1.2 m from left wall, 0.9 m from position 1
4	1.15 m from right wall, 0.9 m from position 2
5	1.8 m from left wall, 1.2 m from back wall, 1 m diagonally from positions 3 and 4

where $\langle\ \rangle$ = average of the scattering parameter over the total number of measured samples (defined in Table 1.2), S_{21} = transmission coefficient, η_{REF} = known reference efficiency. One of the ports was always connected to the transmitting antenna, while another port was connected to the receiving antenna. The reflection coefficients, denoted as S_{22} in (1.5) are not signified as being an average because these parameters were acquired in an anechoic chamber.

Total efficiency (η_{tot}) is defined as the *"Ratio of total radiated power to the power incident on the antenna port."* Mathematically, this is a product of the radiation efficiency and mismatch efficiency, and can be deduced from (1.6).

$$\eta_{tot} = \eta_{rad} \times (1 - (S_{22AUT})^2) \tag{1.6}$$

Note that the reflection coefficient quantities were acquired in an anechoic chamber, hence the omission of the averaging.

It is shown in [47] that efficiency measurements performed using textile antennas on live human beings can be performed in an accurate and controlled manner, with a repeatability sometimes being as close as 2%. The magnitude of on-body losses for a given textile antenna with a small ground plane is seen in this case to be a function of the material properties of that antenna.

1.3.5 Specific Absorption Rate Evaluation

Due to the often very costly measurements caused by the scarcity of certified equipment, the most crucial parameter often investigated with the aid of simulators is the on-body operational safety level, defined in terms of SAR. SAR characterizes the absorption of the radiated electromagnetic energy by the human tissues, and is defined as follows [24]:

$$\text{SAR} = \frac{\sigma \cdot E^2}{\rho} \tag{1.7}$$

where σ (S/m) is the conductivity of the biological material, ρ (kg/m^3) is the material density, and E (V/m) is the electric field strength.

SAR simulations are typically performed in a numerical simulator using a detailed human body model [52]. A very popular model is the Hugo voxel model, which is normally truncated to reduce simulation time. Consistent with practical applications, the antennas are placed at a specific distance from this voxel model to emulate realistic worn placements. Depending on the model's resolution and truncation size, each simulation can easily generate as much as 18–20 million mesh cells, which means that the problem can only be solved using high-performance workstations or graphic processing units (GPUs). A typical simulation setup is shown in Figure 1.11.

An investigation providing information about measurement repeatability and simulation accuracy compared with measurements in various practical scenarios is presented in [55]. A good agreement is obtained, overall of the order of 17%, which is well below the published equipment uncertainty. Measurements are also

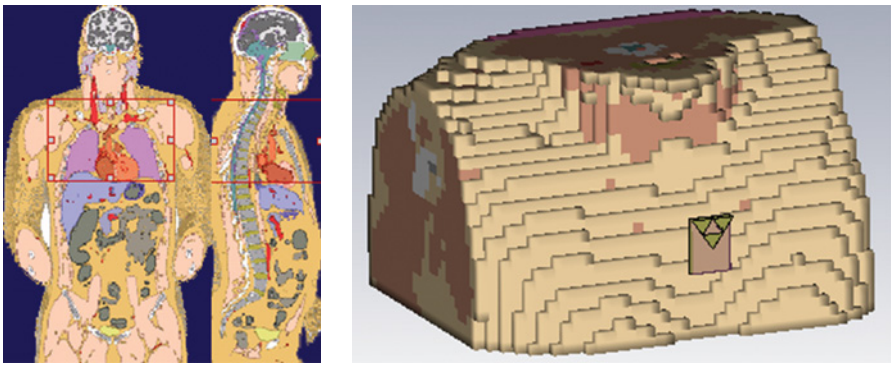

(a) (b)

FIGURE 1.11 SAR simulation setup: (a) Hugo voxel model and (b) AUT placement on the truncated model. *Source:* Soh et al. 2013 [53]. Reproduced with permission of IEEE.

proven to be reproducible with a maximum uncertainty of about 10%. On the other hand, a comparison between the SAR assessed for a flat antenna and several cases of crumpled antennas on a voxel model is presented in Figure 1.12. It is noticed that a higher level of bending results in a higher SAR due to the deeper penetration of the resulting radiation in general. It is worth to note that the resulting average SAR also depends on where the maximum point SAR is located when a detailed model is used in simulations. Lower average SAR can be produced when the antenna is deformed and the radiation penetrates deeper into the body. These lower values are typically located in the fat or muscle layers, which have a lower conductivity. On the contrary, a flat antenna may produce higher SARs, but mainly in the skin layer due to the skin layer's relatively higher conductivity [45].

A commercial DASY-4 system from Schmid & Partner Engineering AG (SPEAG) [56] shown in Figure 1.13 is often utilized to perform SAR measurements. It consists of a measurement server, robot controller, computer, near-field probe, probe alignment sensor, and a specific anthropomorphic mannequin (SAM). The SAM is filled using two tissue-emulating liquids for AUT evaluations at the frequencies of interest. For example, their properties for 2.45 and 5.2 GHz measurements are $\varepsilon_{r2.45} = 39.2$, $\sigma_{2.45} = 1.8$ S/m and $\varepsilon_{r5.2} = 36.0$, $\sigma_{5.2} = 4.66$ S/m, respectively. Prior to AUT measurements, calibrations are performed near the SAM at both frequencies using standard SAR validation dipoles to ensure that the evaluated SAR values are within a specified level. For the cases of 2.45 and 5.2 GHz, they must be below $SAR_{2.45\ GHz} < 6.15$ W/kg and $SAR_{5.2\ GHz} < 5.93$ W/kg [56].

To initialize the measurement, the lineup to the AUT is first connected to a power meter to ascertain that a 100 mW CW signal is fed into the AUTs during subsequent evaluations. The AUT feed cable is secured onto the SAM to ensure a fixed measurement location and to avoid variations due to cable movements. AUTs are placed at a specified distance from the phantom to emulate a realistic practical worn spacing, for instance, a 5 mm thick fleece jacket and another 5 mm air gap modeling the jacket-to-body distance. This additional distance depends on the AUT on-body location and

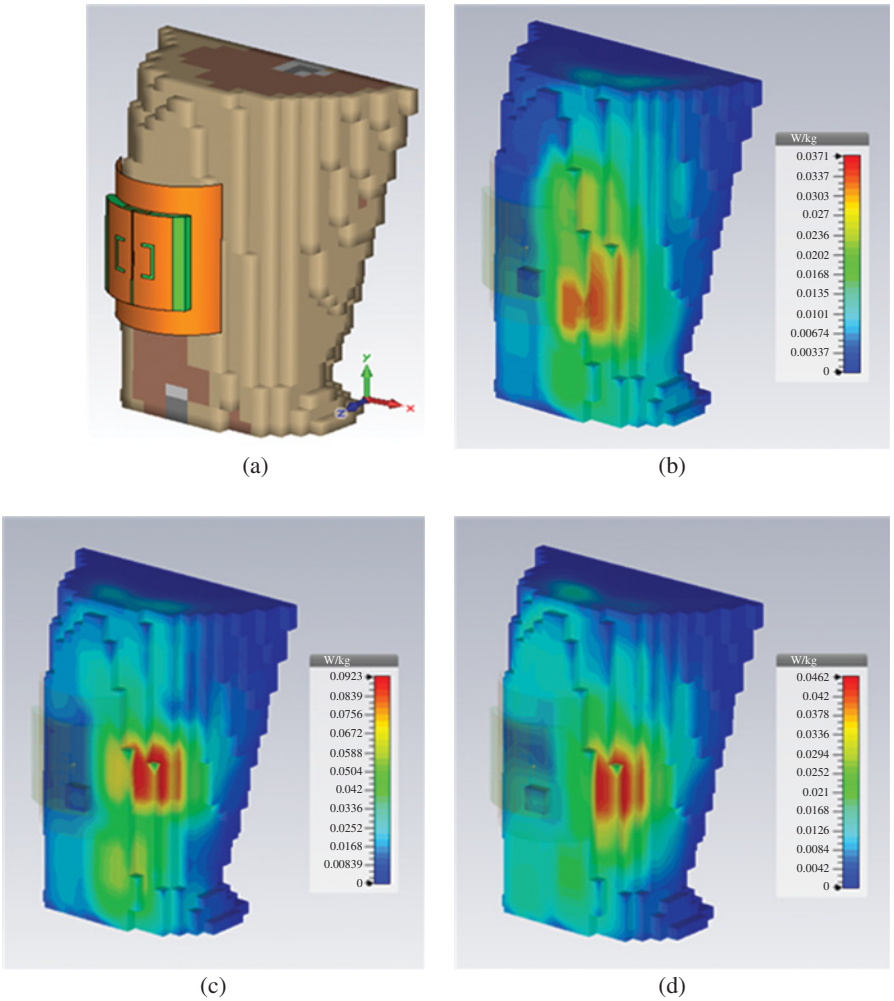

FIGURE 1.12 The SAR of a (a) bent dual-band antenna integrated with an artificial magnetic conductor (AMC) at (b) 2.45 GHz, (c) 5.2 GHz, and (d) 5.8 GHz evaluated on a voxel model. *Source:* Yan et al. 2015 [54]. Reproduced with permission of IEEE. For a color version of this figure, see the color plate section.

the jacket's fitting against the user's body. It is also important to note that the SARs for antennas placed on the body trunk must be evaluated at less than 20 mm distance from a flat phantom [24].

Higher SARs are generally observed when measuring antennas fabricated using conductive textiles with lower conductivities. Further, SAR values are dependent on the distance between the antenna and the phantom. However, these SAR values remain unchanged when the antenna-to-phantom distance approaches 20 mm, along with an increase of the measurement uncertainty. The antenna topology and the size of the ground plane that is shielding the user from the radiation are critical in ensuring

(a) (b)

FIGURE 1.13 SAR measurement setup: (a) top view of the SAM on the DASY-4 system and (b) AUT placement at the measurement location. *Source:* Soh et al. 2013 [53]. Reproduced with permission of IEEE.

that the antenna operates well below the safety limit. Most measured SARs are well below their respective simulated equivalent, indicating that a numerical solver can be used to estimate the worst-case on-body SAR, which is useful to enable a reasonable safety margin in the design phase.

1.3.6 Aging and Varying Environmental Conditions

Just like any conductors, conductive textiles used in antennas are subjected to degradations, either mechanical, electrical, or a combination of both. When implemented on daily clothing, the exposure to washing and cleaning has to be considered. On the other hand, garments for more specialized applications, such as search and rescue, fire-fighting, and the military, require specialized evaluation methods to ensure that the antenna is still fully functional when used under harsh circumstances. For example, in the case of a fire fighter, it is required that the conductive textiles in his garment are as fire retardant as the original apparel, whereas for search and rescue in a maritime environment, they need to be water resistant. As a consequence, dedicated methods to embed or protect the antennas need to be introduced so that they meet their requirements.

In [57], the authors performed an evaluation of the possible factors in the fabrication process that may degrade the usage life of the antenna. The epoxy curing process used and environmental factors may cause water to be trapped in the antenna substrate, resulting in resonant frequency and bandwidth changes. Besides that, textile antennas also experience a decrease in conductivity due to oxidation. To assess both factors, the reflection coefficients of the antennas were measured in a predefined time schedule: just after the time of fabrication, and after a few days, a month, and 2 months. Two fabrication process types were also evaluated: Flectron electrotextile was either stitched and glued, or secured onto the substrate using adhesive sheets. In both cases, it was noticed that a slight resonant frequency shift occurred, without compromising however, the operation in the intended design band, see Figure 1.14.

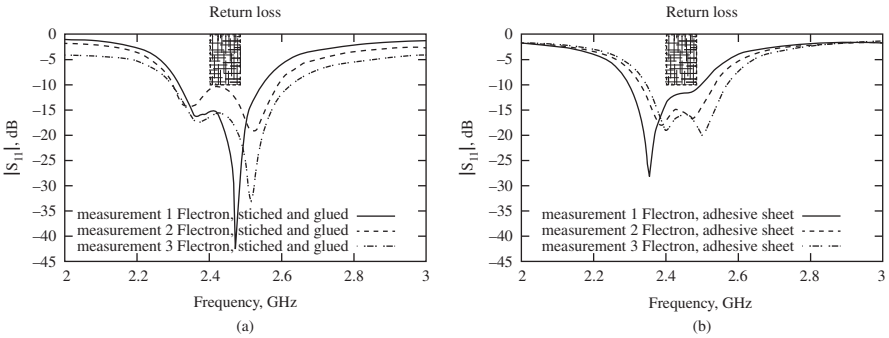

FIGURE 1.14 Reflection coefficients of the Flectron prototypes evaluated over time: (a) prototype fabricated using glueing and stitching, and (b) prototype with adhesive sheet. *Source:* Tronquo et al. 2006 [57]. Reproduced with permission of IEEE.

Several other investigations were also performed to evaluate the effect of different fabrication steps. In [58], the accuracy of manually fabricating a 0.2 mm gap in a co-planar waveguide (CPW) line is investigated. For the first prototype, the CPW line-radiator structure and the ground plane structure are cut individually before being secured onto the fleece. The best effort is put in accurately forming the required 0.2 mm gap by means of manual measurement. The alternative method is to cut an overall CPW–radiator–ground plane structure and securing it first onto the substrate. The gap between the feed line and the ground plane is then cut away after fastening to create the CPW line. The fabrication steps used for the second antenna prototype resulted in a better performance in terms of similarity with simulations.

The investigation in [42] assesses the effects of moisture and freezing a wearable antenna, in addition to the usual bending and on-body coupling investigations. The antenna is made of copper tape and fleece as the conductor and substrate, respectively. The influence of moisture was quantified as the percentage of water in the total mass of the antenna, which was measured using a 0.01 g technical balance. Water was applied to the antenna using a sprinkler and the antenna was gradually dried using a hairdryer. The reflection coefficient was measured after each minute of drying, and it was found that a relative humidity of 10% was sufficient to considerably shift the resonant frequency downward. As a consequence, it is suggested that such antennas need to be water-proofed by using coating for extreme weather conditions. On the other hand, antenna freezing can be expected when such antennas are to be operated by search and rescue teams. In the related investigation, the antenna was first covered using nylon superstrate to avoid moisture. The antenna was then immersed into water and frozen, prior to reflection coefficient measurements. Afterward, it was immersed into a pot of boiling water for 2 minutes before being measured for the second time. It was noticed that the water still penetrated into the substrate despite having the nylon superstrate, thus rendering the antenna unusable.

A comprehensive evaluation of non-conductive textiles is performed in [59]. First, a transmission line method is used to extract the measured scattering parameters of two copper microstrip lines. They are made of a stack of Cordura sheets

attached using a pressure sensitive adhesive. The temperature is varied from −20°C to 40°C and the relative humidity from 10% to 95%. Similarly as in the previous investigation, it is noticed that the observed permittivity and loss tangent behavior follow the changes in relative humidity, which then relates to the absorbed water in the fabric mass. Another aspect of assessment in this work is related to a protective cover for the antenna. The investigation found that surface contamination may be a cause of failure of fabric water-proofing. The two possible factors are explained as follows. First, if the water repellence is chemically added to the fabric, a strong salt solution can wash the added layer away. Secondly, user comfort includes the breathability factor; thus, small holes are introduced to enable water evaporation. These holes are impenetrable by water due to the surface tension. However, salt lowers the surface tension of water rendering salt water to be penetrable into many waterproof fabrics.

In [60], the effect of several washing and drying cycles based on the ISO 6330:2000 and ISO 139 standards, respectively, was investigated for an inset-fed microstrip patch antenna. The washing temperature was set at 30 ± 3°C, and the samples were placed in a room at a temperature of 23 ± 2°C and humidity of 50 ± 4 % upon drying. The textile was considered dried when weighing performed in intervals of 2 hours indicated no change in mass greater than 0.25%. Measurements of the antenna made using Flectron and Electrodag and covered with a breathable thermoplastic polyurethane (TPU) layer were performed after one, three, and six washing cycles. With the increase in the number of washing cycles, the antenna based on Flectron was observed to degrade in terms of radiation efficiency and matching, thus resulting in resonance shifting. This is believed to be due to mechanical delamination and detachment from the substrate. Besides that, the Flectron layer itself suffered deterioration in terms of resistivity to a value of about 1.2 Ω/sq, resulting in the observed efficiency decrease despite still being within acceptable limits. On the contrary, the antennas based on the Electrodag displayed a more stable performance in terms of matching and efficiency.

1.4 CONCLUSION

In this chapter, the design, development, and evaluation procedures for textile antennas have been presented. Since these materials are either newly introduced or have been traditionally used for other purposes, for example, EMI shielding or grounding, one of the important and yet challenging aspects in the field of textile antennas is to properly characterize the electrical properties of these materials at the intended frequencies. Basically, two types of materials to realize textile antennas are discussed, conductive and non-conductive textiles.

First, a simple and pragmatic, but at the same time, efficient and result-oriented procedure to design and fabricate textile antennas using commercially available textiles and flexible conductive layers has been proposed and described. This simple procedure utilizes manual fabrication tools. The accuracy of the produced prototypes, verified across the various antennas operating in distinct frequency bands is satisfactory, with an accuracy of 0.2 mm. A general top-level design guideline

and its limitations are also presented. Since a classical soldering technique, as used in fabricating conventional antennas, might not always be applicable for conductive textiles, there is a need for alternatives such as the use of conductive epoxy.

Next, procedures to verify the performance of flexible/textile antennas have been presented. Most of the procedures are adapted versions of the evaluation procedures used for conventional, rigid antennas. In contrast to the general on-head or in-hand evaluations performed for handset antennas, which are already widely available in the literature, evaluation of textile antennas has been mainly focusing on the upper human torso or the arms. Additional tools to characterize and properly validate these antennas and measures to keep the performance stable have been outlined in this chapter. Since the major practical issues when using textile antennas are the bandwidth detuning and power absorption when operating in the vicinity of a user, a crucial aspect is the use of on-body evaluation methods. Antenna performance is assessed in the proximity of either a human user or a phantom and must lead to sufficient design information to guarantee this performance in the simulation-based design process, where the proximity of the human body also has to be taken into account. Minor steps such as the use of a fleece jacket and spacers, properly applied, aim at providing a better measurement accuracy and consistency when evaluating textile antennas. The typical small antenna-to-body distance also causes safety concerns. This chapter has also addressed this issue, with a fundamental study on SAR.

REFERENCES

[1] P. S. Hall and Y. Hao, *Antennas and Propagation for Body-Centric Wireless Communications*, 2nd ed. Artech House, Norwood, MA, 2012.

[2] P. J. Soh, G. A. E. Vandenbosch, X. Chen, P.-S. Kildal, S. L. Ooi, and H. Aliakbarian, "Wearable Textile Antenna Efficiency Characterization using a Reverberation Chamber," in IEEE International Symposium on Antennas and Propagation, New York, July 3–8, 2011, pp. 810–813.

[3] M. A. R. Osman, M. K. A. Rahim, M. Azfar, N. A. Samsuri, F. Zubir, and K. Kamardin, "Design, implementation and performance of ultra-wideband textile antenna," *Prog. Electromagnetics Res. B*, vol. 27, pp. 307–325, 2011.

[4] C. Hertleer, H. Rogier, L. Vallozzi, and L. V. Langenhove, "A textile antenna for off-body communication integrated into protective clothing for firefighters," *IEEE Trans. Antennas Propag.*, vol. 57, no. 4, pp. 919–925, April 2009.

[5] E. C. Lee, P. J. Soh, N. B. M. Hashim, G. A. E. Vandenbosch, H. Mirza, I. Adam, and S. L. Ooi, "Design of a Flexible Minkowski-like Pre-fractal (MLPF) Antenna with Different Ground Planes for VHF LMR," in 2011 International Workshop on Antenna Technology (iWAT), Hong Kong, March 7–9, 2011, pp. 298–301.

[6] E. C. Lee, P. J. Soh, N. B. M. Hashim, G. A. E. Vandenbosch, V. Volski, I. Adam, and M. Z. A. A. Aziz, "Design and Fabrication of a Flexible Minkowski Fractal Antenna for VHF Applications," in Proceedings of the 5th European Conference on Antennas and Propagation, Rome, April 11–15, 2011, pp. 521–524.

[7] P. Salonen and L. Hurme, "A Novel Fabric WLAN Antenna for Wearable Applications," in IEEE Antennas and Propagation Society International Symposium, 2003, Columbus, OH, June 22–27, 2003, pp. 700–703.

[8] "Introduction to the Cospas-Sarsat System," International Cospas-Sarsat Programme, 2009.

[9] S. Sankaralingam and B. Gupta, "Use of electro-textiles for development of wibro antennas," *Prog. Electromagnetics Res. C*, vol. 16, pp. 183–193, 2010.

[10] N. H. M. Rais, P. J. Soh, F. Malek, R. B. Ahmad, N. B. M. Hashim, and P. S. Hall, "A Review of Wearable Antennas," in Loughborough Antennas and Propagation Conference (LAPC), Loughborough, November 16–17, 2009, pp. 225–228.

[11] P. J. Soh, G. A. E. Vandenbosch, S. L. Ooi, and H. M. R. Nurul, "Characterization of a plain broadband textile PIFA," *Radioeng.*, vol. 20, no. 4, pp. 718–725, December 2011.

[12] P. J. Soh, G. A. E. Vandenbosch, S. L. Ooi, and N. H. M. Rais, "Design of a broadband all-textile slotted PIFA," *IEEE Trans. Antennas Propag.*, vol. 60, no. 1, pp. 379–384, January 2012.

[13] P. J. Soh, G. A. E. Vandenbosch, V. Volski, and H. M. R. Nurul, "Characterization of a Simple Broadband Textile Planar Inverted-F Antenna (PIFA) for On Body Communications," in International Conference on Applied Electromagnetics and Communication, Dubrovnik, Croatia, September 20–23, 2010, pp. 1–4.

[14] C. Hertleer, A. Tronquo, H. Rogier, L. Vallozzi, and L. V. Langenhove, "Aperture-coupled patch antenna for integration into wearable textile systems," *IEEE Antennas Wireless Propag. Lett.*, vol. 6, pp. 392–395, 2007.

[15] "Specification Sheet—ShieldIt Super," LessEMF Inc., 2015.

[16] "Specification Sheet—Pure Copper Polyester Taffeta Fabric," LessEMF Inc., 2015.

[17] "Specification Sheet—Felt Sheet 6 mm," RS Components Inc., 2015.

[18] T. F. Kennedy, P. W. Fink, A. W. Chu, N. J. Champagne, G. Y. Lin, and M. A. Khayat, "Body-worn E-textile antennas: the good, the low-mass, and the conformal," *IEEE Trans. Antennas Propag.*, vol. 57, no. 4, pp. 910–918, April 2009.

[19] I. Locher, M. Klemm, T. Kirstein, and G. Troster, "Design and characterization of purely textile patch antennas," *IEEE Trans. Adv. Packag.*, vol. 29, no. 4, pp. 777–788, November 2006.

[20] "Polar Fleece," Wikipedia, 2015.

[21] "Specification Sheet—Fleece Jacket," RS Components Inc., 2015.

[22] P. Salonen, Y. Rahmat-Samii, and M. Kivikoski, "Wearable Antennas in the Vicinity of Human Body," in IEEE Antennas and Propagation Society International Symposium, June 20–25, 2004, pp. 467–470.

[23] A. Tronquo, H. Rogier, C. Hertleer, and L. V. Langenhove, "Robust planar textile antenna for wireless body LANs operating in 2.45 GHz ISM band," *Electron. Lett.*, vol. 42, no. 3, pp. 142–143, February 2006.

[24] "Human Exposure to Radio Frequency Fields from Hand-held and Body-mounted Wireless Communication Devices–Human Models, Instrumentation and Procedures IEC 62209 Standard," The International Electrotechnical Commission (IEC), 2010.

[25] T. Weiland, "A discretization method for the solution of Maxwell's equations for six-component fields," *AEÜ - Int. J. Electron. Commun.*, vol. 31, no. 3, p. 116, 1977.

[26] T. Weiland, "Time domain electromagnetic field computation with finite difference methods," *Int. J. Numer. Model., Electron. Netw. Devices Fields*, vol. 9, no. 4, pp. 295–319, 1996.

[27] K. Yee, "Numerical solution of initial boundary value problems involving Maxwell's equations in isotropic media," *IEEE Trans. Antennas Propag.*, vol. 14, no. 3, pp. 302–307, May 1996.

[28] A. Taflove and S. C. Hagness, *Computational Electrodynamics: The Finite-Difference Time-Domain Method*, 3rd ed. Artech House, Norwood, MA, 2005.

[29] F. Zheng, Z. Chen, and J. Zhang, "A finite-difference time-domain method without the Courant stability conditions," *IEEE Microw. Guid. Wave Lett.*, vol. 9, no. 11, pp. 441–443, August 1999.

[30] E. Li, I. Ahmed, and R. Vahldieck, "Numerical dispersion analysis with an improved LOD–FDTD method," *IEEE Microw. Guided Wave Lett.*, vol. 17, no. 5, pp. 319–321, April 2007.

[31] P. B. Johns and R. L. Beurle, "Numerical solution of 2-dimensional scattering problems using a transmission-line matrix," *Proc. Inst. Electrical Eng.*, vol. 11, no. 9, pp. 1203–1208, September 1971.

[32] C. Christopoulos, *The Transmission-Line Modeling Method: TLM*. Wiley-IEEE Press, Piscataway, NJ, 1996.

[33] J.-M. Jin, *The Finite Element Method in Electromagnetics*, 2nd ed. Wiley-IEEE Press, Piscataway, NJ, 2002.

[34] A. Bossavit, *Computational Electromagnetism: Variational Formulations, Complementarity, Edge Elements*. Academic Press, New York, 1997.

[35] R. F. Harrington, *Field Computation by Moment Methods*. Wiley-IEEE Press, Piscataway, NJ, 1993.

[36] C. A. Balanis, *Antenna Theory Analysis and Design*, 3rd ed. John Wiley & Sons, New York, 2005.

[37] N. Chahat, M. Zhadobov, R. Sauleau, and K. Ito, "A compact UWB antenna for on-body applications," *IEEE Trans. Antennas Propag.*, vol. 59, no. 4, pp. 1123–1131, April 2011.

[38] P. Samal, P. J. Soh, and G. A. E. Vandenbosch, "UWB all-textile antenna with full ground plane for off-body WBAN communications," *IEEE Trans. Antennas Propag.*, vol. 62, no. 1, pp. 102–108, January 2014.

[39] Z. Wang, L. Z. Lee, D. Psychoudakis, and J. L. Volakis, "Embroidered multiband body-worn antenna for GSM/PCS/WLAN communications," *IEEE Trans. Antennas Propag.*, vol. 62, no. 6, pp. 3321–3329, March 2014.

[40] P. J. Soh, S. J. Boyes, G. A. E. Vandenbosch, Y. Huang, and S. L. Ooi, "On-body characterization of dual-band all-textile PIFAs," *Prog. Electromagn. Res.*, vol. 129, pp. 517–539, July 2012.

[41] Q. Bai and R. Langley, "Wearable EBG Antenna Bending and Crumpling," in Loughborough Antennas and Propagation Conference (LAPC), Loughborough, November 16–17, 2009, pp. 201–204.

[42] B. Ivsic, G. Golemac, and D. Bonefacic, "Performance of Wearable Antenna Exposed to Adverse Environmental Conditions," in 21st International Conference on Applied Electromagnetics and Communication (ICECom), Dubrovnik, Croatia, October 14–16, 2013, pp. 1–5.

[43] P. J. Soh, B. van den Bergh, H. Xu, H. Aliakbarian, S. Farsi, P. Samal, G. A. E. Vandenbosch, D. M. M.P. Schreurs, and B. K. J. C. Nauwelaers, "A smart wearable textile antenna system for biomedical telemetry system," *IEEE Trans. Microw. Theory Tech.*, vol. 61, no. 5, pp. 2253–2261, May 2013.

[44] J. Choi, J. Tak, and S. Lee, "All-textile higher order mode circular patch antenna for on-body to on-body communications," *IET Microw. Antennas Propag.*, vol. 9, no. 6, pp. 576–584, April 2015.

[45] N. A. Elias, N. A. Samsuri, M. K. A. Rahim, and N. Othman, "Investigation of Crumpling Effects on EM Absorption and Antenna Performance at 2.4 GHz," in 2013 IEEE International RF and Microwave Conference (RFM), Penang, Malaysia, December 9–11, 2013, pp. 395–399.

[46] S. Boyes, Y. Huang, N. Khiabani, P. J. Soh, and G. A. E. Vandenbosch, "Repeatability and Uncertainty Evaluations of On-body Textile Antenna Efficiency Measurements in a Reverberation Chamber," in 2012 Loughborough Antennas and Propagation Conference (LAPC), Loughborough, UK, November 12–13, 2012, pp. 1–5.

[47] S. J. Boyes, P. J. Soh, Y. Huang, G. A. E. Vandenbosch, and N. Khiabani, "On-body performance of dual-band textile antennas," *IET Microw. Antennas Propag.*, vol. 6, no. 15, pp. 1696–1703, December 2012.

[48] S. J. Boyes, P. J. Soh, Y. Huang, G. A. E. Vandenbosch, and N. Khiabani, "Measurement and performance of textile antenna efficiency on a human body in a reverberation chamber," *IEEE Trans. Antennas Propag.*, vol. 6, no. 2, pp. 871–881, February 2013.

[49] K. Rosengren and P.-S. Kildal, "Study of distributions of modes and plane waves in reverberation chambers for the characterization of antennas in a multipath environment," *Microw. Opt. Technol. Lett.*, vol. 30, no. 6, pp. 386–391, September 2001.

[50] P.-S. Kildal and C. Carlsson, "Detection of a polarization imbalance in reverberation chambers and how to remove it by polarization stirring when measuring antenna efficiencies," *Microw. Opt. Technol. Lett.*, vol. 34, no. 2, pp. 145–149, July 2002.

[51] P.-S. Kildal, X. Chen, C. Orlenius, M. Franzen, and C. S. L. Patane, "Characterization of reverberation chambers for OTA measurements of wireless devices: physical formulations of channel matrix and new uncertainty formula," *IEEE Trans. Antennas Propag.*, vol. 60, no. 8, pp. 3875–3891, August 2012.

[52] "CST Microwave Studio," Darmstadt, Germany: CST-Computer Simulation Technology AG, 2015.

[53] P. J. Soh, G. A. E. Vandenbosch, F. H. Wee, A. van den Bosch, M. Martinez-Vazquez, and D. Schreurs, "Specific Absorption Rate (SAR) Evaluation of Biomedical Telemetry Textile Antennas," in 2013 IEEE MTT-S International Microwave Symposium Digest (IMS), Seattle, WA, June 2–7, 2013, pp. 1–4.

[54] S. Yan, P. J. Soh, and G. A. E. Vandenbosch, "Dual-band textile MIMO antenna based on substrate integrated waveguide (SIW) technology," *IEEE Trans. Antennas Propag.*, vol. 63, no. 11, pp. 4640–4647, November 2015.

[55] P. J. Soh, G. A. E. Vandenbosch, F. H. Wee, A. van den Bosch, M. Martinez-Vazquez, and D. Schreurs, "Specific absorption rate (SAR) evaluation of textile antennas," *IEEE Antennas Propag. Mag.*, vol. 57, no. 2, pp. 229–240, April 2015.

[56] "DASY-4 V4.7 System Handbook," Schmid & Partner Engineering AG, 2008.

[57] A. Tronquo, H. Rogier, C. Hertleer, and L. V. Langenhove, "Applying Textile Materials for the Design of Antennas for Wireless Body Area Networks," in First European Conference on Antennas and Propagation (EuCAP), Nice, France, 2006, pp. 1–5.

[58] P. J. Soh, G. A. E. Vandenbosch, and J. Higuera-Oro, "Design and Evaluation of Flexible CPW-fed Ultra Wideband (UWB) Textile Antennas," in 2011 IEEE International RF and Microwave Conference (RFM), Seremban, Negeri Sembilan, December 12–14, 2011, pp. 133–136.

[59] J. Lilja, P. Salonen, T. Kaija, and P. d. Maagt, "Design and manufacturing of robust textile antennas for harsh environments," *IEEE Trans. Antennas Propag.*, vol. 60, no. 9, pp. 4130–4140, September 2012.

[60] M. L. Scarpello, I. Kazani, C. Hertleer, H. Rogier, and D. V. Ginste, "Stability and efficiency of screen-printed wearable and washable antennas," *IEEE Antennas Wireless Propag. Lett.*, vol. 11, pp. 838–841, July 2012.